Available online at www.sciencedirect.com
ScienceDirect
Journal of Hydrodynamics
www.sciencedirect.com/
science/journal/10016058

Significant Intervals of Energy Transforms in Bubbles Freely Oscillating in Liquids

Karel Vokurka
Physics Department, Technical University of Liberec
Liberec, Czech Republic
E-mail: karel.vokurka@tul.cz

ABSTRACT

A wall motion of a bubble freely oscillating in a liquid is studied from the point of view of energy conversions at different instants. It is shown that the time of the bubble oscillation can be divided into two distinct intervals. In the first long interval (here called PK and KP intervals) the prevailing energy conversion is between the potential energy of the bubble and the kinetic energy of the liquid. In the second short interval (here called KI and IK intervals) the kinetic energy of the liquid is transformed into the internal energy of the gas/vapor in the bubble interior and into some other forms of energies. It is shown that by observing the bubble wall motion in the PK and KP intervals, only the value of the maximum bubble radius in the corresponding oscillation can be determined. However, only the knowledge of the maximum bubble radii is insufficient for formulation of a correct theoretical model. Unfortunately this fact is often not respected in the literature.

KEY WORDS: Free bubble oscillations; energy conversions in bubbles

INTRODUCTION

Bubble oscillations remain an important topic in fluid dynamics. While they are traditionally associated with erosion damage [1 - 5], recent efforts are aiming at medical applications, such as contrast-enhancing in ultrasonic imaging [6 - 9] and shock wave lithotripsy [10, 11]. Further recent studies are aiming at seismic airgun development [12 - 14], acoustic emission monitoring [15], bubble augmented waterjet propulsion [16], study of liquid compressibility [17], microbubble dynamics monitoring [18], standing cavitation bubbles generation [19], and optimization of an augmented Prosperetti-Lezzi model [20]. In experimental studies of free bubble oscillations both spark generated bubbles [1, 21 – 25] and laser generated bubbles [2, 3, 26 – 33] represent very useful tools.

In spite of many works dealing with physics of bubble oscillations (for a recent extensive review of this topic see, e.g. [34]), there still remain many unanswered questions. One important point concerns energy transforms in oscillating bubbles. Analyses of energy transforms either theoretical, or even based on experimental data, are rare in literature and an analysis of energy transforms encompassing different time intervals is missing completely. This has serious consequences. For example, when reviewing the literature it can be seen that many authors fit their experimental radius vs. time data with theoretical variations computed using models based on an assumption of an ideal gas bubble oscillating adiabatically. After selecting a suitable intensity of the bubble oscillation the correspondence over a relatively large part of the time of the bubble oscillation can be obtained. The theoretical model is thus considered to be validated and is further

used to compute, e.g., pressure and temperature in the bubble at its maximum contraction. As will be shown, such an approach, which at first sight might seem to be correct, leads to incorrect results.

In Section 1 a radius time history of an experimental bubble is first compared with theoretical computations. It is shown that during a predominant part of the time of the bubble contraction all commonly used theoretical models fit the experimental data with almost the same accuracy. To explain this surprising correspondence between the models and the experiment, energy conversions in a freely oscillating bubble are analyzed in Section 2. In Section 3 the results of the analysis are discussed and an attention is drawn to the pitfalls that can be encountered when interpreting the experimental data.

EXPERIMENT VS. THEORY

As an introduction to the following discussion, selected experimental results are compared with theoretical ones in this Section. The experimental data have been obtained when studying the spark generated bubbles. These bubbles have been produced by discharging a capacitor bank via a sparker submerged in a laboratory water tank having dimensions of 6 m (length) x 4 m (width) x 5.5 m (depth). The sparker electrodes have been made of tungsten wires of diameter 1 mm and the gap between the two electrodes has been set at approximately 1 mm. The sparker has been positioned at a depth of 2.5 m with a distance to the nearest water tank wall of 1.2 m. The capacitance of the capacitor bank could be varied in steps by connecting 1 to 10 capacitors in parallel. Each of these capacitors had a capacitance of 40 μF. The capacitors have been charged from a high voltage source whose voltage could be varied from 2.0 to 2.5 kV. An air-gap switch has been used to trigger the discharge through the sparker.

Both the spark discharge and subsequent bubble oscillations are accompanied by intensive optic and acoustic radiations. These radiations have been monitored by a broadband hydrophone and an optic detector. A limited number of high-speed camera records have been also taken with framing rates ranging from 2800 to 3000 fps (frames/second). A more detailed description of the experimental setup can be found in [35 - 37].

The size of the bubbles studied in these experiments is described by the first maximum radius R_{M1}, and the bubble oscillation intensity is described by the non-dimensional peak pressure in the first acoustic pulse $p_{zp1}=(p_{p1}.r)/(p_{\infty}.R_{M1})$ [36]. Here p_{p1} is the peak pressure in the first acoustic pulse $p_1(t)$, that has been radiated by the bubble during its first contraction, p_{∞} is the ambient (hydrostatic) pressure at the place of the sparker, and r is the hydrophone distance from the sparker center.

In the following the results from one particular experiment will be described. In this experiment the bubble size was R_{M1}=51.5 mm, the hydrophone distance from the sparker center was r=0.5 m, and the intensity of this bubble oscillation, as determined from the pressure record, was p_{zp1}=70.3. Selected frames from a film record obtained by a high-speed camera and showing the bubble at different instants during the first contraction phase are shown in Fig. 1. Throughout this paper this bubble will be used as a reference.

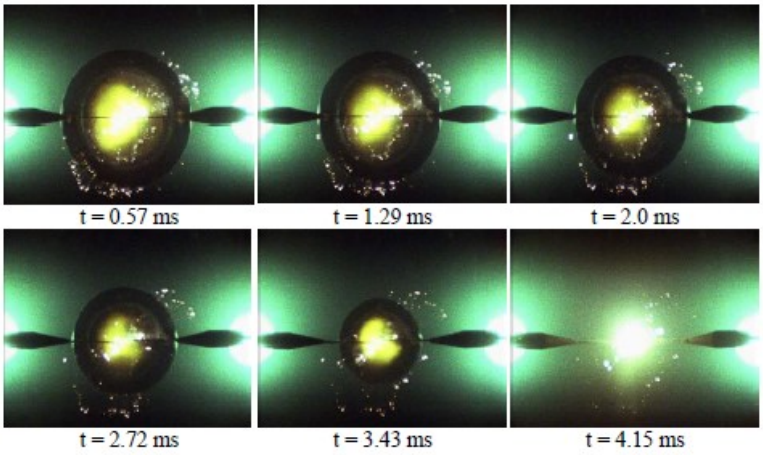

Fig. 1 Selected frames from a high-speed camera record. The bubble size is R_{M1}=51.5 mm, the intensity of bubble oscillation is p_{zp1}=70.3, the framing rate is 2800 fps. The time at each frame refers to the time scale origin, which has been selected to coincide with a time, when the bubble attains the maximum radius R_{M1} (see also Fig. 2). At the sides of the bubble two conical brass holders of the tungsten electrodes can be seen. The tungsten electrodes themselves can be seen penetrating into the bubble. Small bright objects with tube like traces moving outside the bubble are plasma packets. The two bright objects at the sides of the frames are illuminating lamps.

The bubble radii corresponding to different instants can be determined from the frames. Values of the bubble radii obtained in this way are displayed in Fig. 2. As the experimental bubble is not ideally spherical (it is slightly elongated in a vertical direction), the data points represent an average from two perpendicular directions (horizontal and vertical). The time interval between two points is given by the framing rate of the camera.

In Fig. 2 the experimental points are plotted together with theoretical variations of the bubble radius R with time t. The theoretical variations have been computed using four different bubble models. One of these theoretical curves has been obtained under assumption of a non-compressible liquid (that is, using the Rayleigh's model [39]). The remaining three curves have been computed under assumption of liquid compressibility using the Gilmore's, Herring's, and Herring's modified model [39]. In all theoretical models a spherical gas bubble oscillating adiabatically has been assumed. The constants used in these computations had the values corresponding to the experimental conditions: the ambient pressure p_∞=125 kPa, liquid density ρ=10^3 kg.m^{-3}, velocity of sound in the liquid c_∞=1480 m.s^{-1}, the ratio of the specific heats of the gas in the bubble γ=1.25, constants in the Tait equation of state for the liquid B=300 MPa and n=7, the bubble size R_{M1}=51.5 mm, and the non-linear amplitude of the first bubble oscillation A_1=2.72 (the non-linear amplitude is defined as A_1=R_{M1}/R_e, where R_e is an "equilibrium" radius). The value of A_1 has been determined from the experimental value of p_{zp1}=70.3 using the theoretical scaling function A_1=$f(p_{zp1},\gamma)$ and the procedure described in Ref. [36].

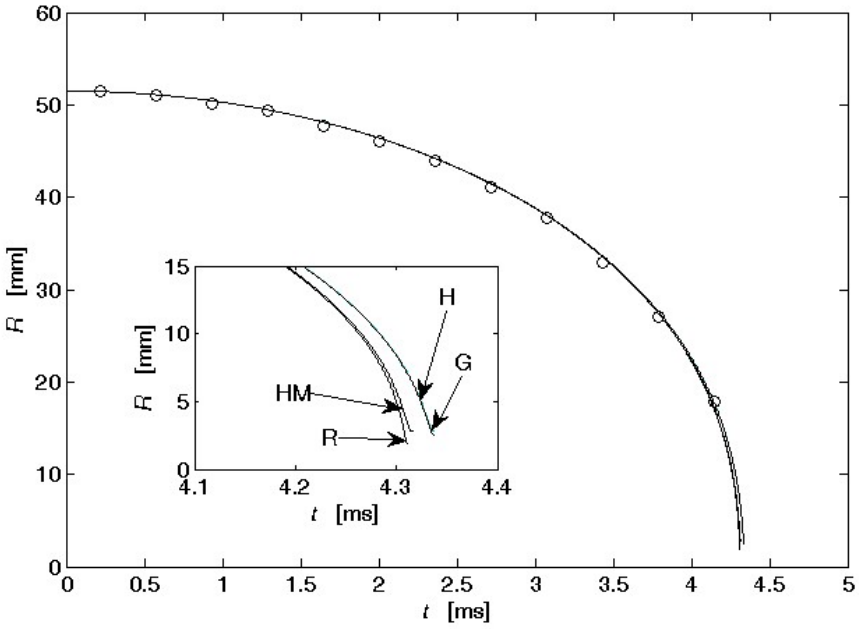

Fig. 2 Comparison of the experimental data with theoretical variations of the bubble radius R with time t during the first contraction phase (experimental data for the following expansion phase originating from the same experiment are shown in Fig. 4). The time scale origin has been selected as an instant when the theoretical computations start, i.e., when the bubble radius is $R=R_{MI}$, and the bubble wall velocity $dR/dt=0$. The experimental points have then been shifted along the time scale until the best agreement with the theoretical curves has been obtained. The position of the first data point then determines a time reference for the remaining experimental points. The final stages of the bubble contraction are shown enlarged in the inset. Letters HM, R, H, and G stand for Herring's modified, Rayleigh's, Herring's, and Gilmore's models respectively

As can be seen in Fig. 2 at first sight, all theoretical models yield a reasonable fit to the experimental points. Even more, the curves corresponding to different theoretical models are almost indistinguishable mutually in the scales used in Fig. 2. The overall shapes of the theoretical curves *R(t)* resemble an "inverted tea cup" (in Fig. 2 only a half of this "cup" is displayed), and from what has been said it follows that this shape is independent of the form of the equations used to approximate the liquid compressibility. Or, in other words, it is independent of the theoretical model used in computations. The theoretical curves start to differ from each other only at the final stages of the bubble contraction (shown enlarged in the inset), where, unfortunately, no experimental points are available for comparison. To explain this relative independence of the *R(t)* curve shape on the liquid compressibility, the transforms of energies in a freely oscillating bubble must be analyzed. This will be done in the following Section.

INTERVALS OF ENERGY TRANSFORM

In the experiments described in Section 1 the spark generated bubbles have been studied. As it has been shown earlier by analyzing the radiated pressure waves [38], the spark generated bubbles are basically vapor bubbles (that is, except that the bubble contains a limited amount of gases, the vapor evaporation and condensation at the bubble wall play an important role for them), they do not behave adiabatically [37], and their oscillations are accompanied by certain energy transforms, character of which is still not very well understood [35 - 37]. At present time there is no theoretical model available in the literature taking into account all these features. Therefore Herring's modified model will be used here. This model has an advantage in a relatively high acoustic radiation and is relatively simple so that the analysis is more transparent. It will be shown later that this model meets the expectations of its role in this paper well.

The model assumes a spherical gas bubble freely oscillating in a compressible and extended liquid. The thermal behavior of the bubble is assumed to be adiabatic. The excitation of the bubble for free oscillation is assumed to be done by initially decreasing its energy. The analysis will be limited to the first contraction and expansion phases. It will be shown that even if this simple model is used to represent a real spark generated bubble, a useful insight into the transforms of energies can be obtained.

Consider a spherical gas bubble of radius R_{M1} and let the bubble be initially at rest. At the moment t=0, the pressure of the gas in the bubble interior is instantaneously decreased to a value $P_{m1}<p_\infty$. Due to the excess pressure, p_∞ - P_{m1}, the bubble will start contracting to a first minimum radius R_{m1} (the first contraction phase lasting T_{c1}), and then will expand to a second maximum radius R_{M2} (the first expansion phase lasting T_{e1}).

The initial potential energy of the bubble is

$$E_{pM1} = \frac{4}{3}\pi p_\infty R_{M1}^3 \quad . \tag{1}$$

During the contraction from R_{M1} to R the decrease of the potential energy equals

$$\Delta E_p = E_{pM1} - E_p = \frac{4}{3}\pi p_\infty \left(R_{M1}^3 - R^3\right) \quad . \tag{2}$$

The liquid, which was initially at rest, is streaming towards the bubble during the contraction phase and acquires a kinetic energy

$$E_k = 2\pi\rho_\infty \dot{R}^2 R^3 \quad , \tag{3}$$

where the dot denotes a time derivative.

As said above, during the bubble contraction and expansion the gas pressure, P, is supposed to change according to the adiabatic law

$$P = P_{m1}\left(\frac{R_{M1}}{R}\right)^{3\gamma} \quad . \tag{4}$$

The initial internal energy of the gas (referred to an infinite expansion of the bubble, at which the internal energy is defined to be zero) is

$$E_{im1} = \frac{4}{3}\pi \frac{1}{\gamma - 1} P_{m1} R_{M1}^3 \quad . \tag{5}$$

The work done on the gas during the compression from R_{M1} to R will manifest itself as the increase of the internal energy

$$\Delta E_i = E_i - E_{im1} = \frac{4}{3}\pi \frac{1}{\gamma - 1} P_{m1} R_{M1}^3 \left[\left(\frac{R_{M1}}{R}\right)^{3(\gamma-1)} - 1\right] \quad . \tag{6}$$

The oscillation of this bubble is governed by the energy relation

$$\Delta E_p = E_k + \Delta E_i + \Delta E_a \quad , \tag{7}$$

where ΔE_a is a cumulative acoustic energy radiated from the bubble. The acoustic energy ΔE_a can be determined from Eq. (7) after computing ΔE_p, E_k, and ΔE_i from Eqs. (2), (3), and (6).

To determine the energies ΔE_p, E_k, ΔE_i, and ΔE_a, the time variations of R and $\dot{R}$ are needed. In this Section these variations will be determined using the Herring's modified equation [36]

$$R\ddot{R} + \frac{3}{2}\dot{R}^2 = \frac{1}{\rho_\infty}\left[P - p_\infty + \dot{P}\frac{R}{c_\infty} \right] \quad . \tag{8}$$

The pressure P at the bubble wall is given by Eq. (4) and the initial conditions of Eq. (8) are $R(0)=R_{M1}$ and $\dot{R}(0)=0$.

In Eq. (8) the bubble oscillation intensity is determined by the ratio of the initial pressure P_{m1} and the ambient pressure p_∞, that is by $P^*_{m1}=P_{m1}/p_\infty$. However, as shown in [38], in theoretical computations a more convenient intensity measure is the non-linear amplitude of the first oscillation A_1. The "equilibrium" radius R_e used in computing A_1 is defined by a condition that $P=p_\infty$ when $R=R_e$. Then $A_1 = \left(P^*_{m1}\right)^{-1/(3\gamma)}$. Another measure of the bubble oscillation intensity, convenient above all in experimental works, is the non-dimensional peak pressure in the first acoustic pulse, p_{zp1}, introduced already in Section 1.

As said above, in this work the Herring's modified equation (8) has been selected for two reasons. First, it is a relatively simple equation. However, the second reason is even more important. As has been shown in many experiments with spark and laser generated bubbles, cavitation bubbles and bubbles generated by underwater chemical explosions, oscillations of real bubbles are strongly damped. At present, unfortunately, some energy transforms, which are responsible for this damping, are not sufficiently known [3, 26, 35 - 38]. Thus a significant part of the damping, because its nature is not known, is not taken into account in any theoretical computations published in literature. The unknown energy transforms certainly limit the validity of any present theoretical model and thus the results obtained with any model have to be interpreted with extreme caution. Herring's modified equation, when compared with Gilmore's equation, gives a stronger acoustic radiation, and such a stronger acoustic radiation may be used to cover a part of the unknown energy losses. Thus for the same intensity of oscillations Herring's modified equation gives less extreme results, which seems to be closer to reality than the results obtained for the same initial intensity with Gilmore's equation.

An example of computed variations of energies ΔE_p, E_k, ΔE_i, and ΔE_a with time t is given in Fig 3. The variations shown in Fig. 3 are a graphical representation of Eq. (7) and thus ΔE_p represents a decrease of E_p and ΔE_i an increase of E_i. For convenience the energies are displayed in a normalized form defined as $E_z=E/E_{pM1}$. When solving Eqs. (2), (3), (6), and (8) the values of physical constants and of other parameters given in Section 1 have been used.

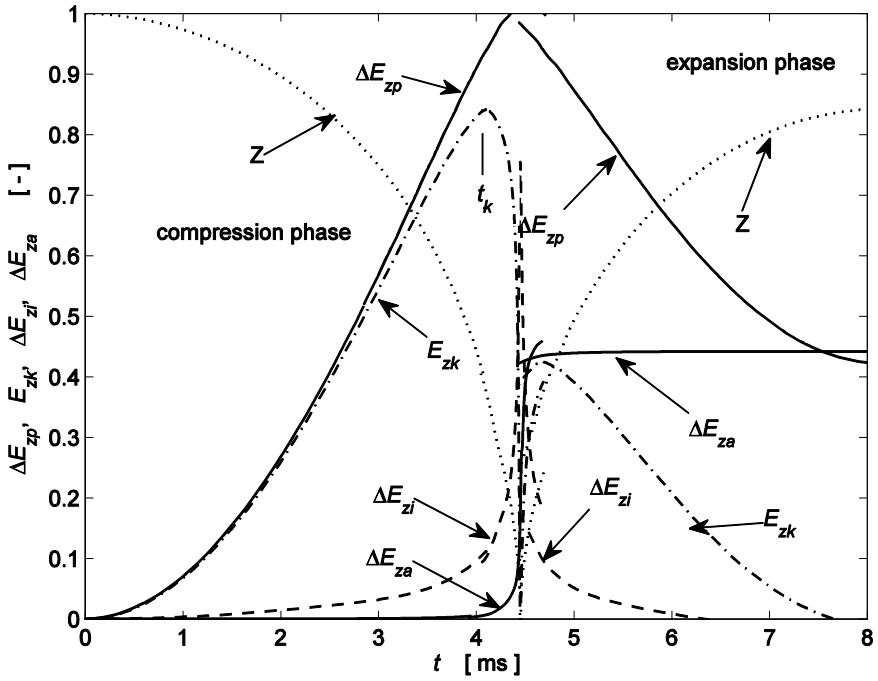

Fig. 3 Variations of the normalized energies ΔE_{zp}, E_{zk}, ΔE_{zi}, and ΔE_{za} with time t in the first contraction (compression) and expansion phases. The contraction phase is lasting T_{c1}, the expansion phase is lasting T_{e1}. Time scale origin was set to coincide with the beginning of the contraction phase. $Z=R/R_{M1}$ is a normalized bubble radius and t_k is an instant, when the kinetic energy E_k attains a maximum value

As can be seen in Fig. 3 the transform of the bubble potential energy into the kinetic energy of the liquid is dominating during almost 97% of the contraction phase. The transform of the potential energy into the internal energy of the gas or into the radiated acoustic energy is not significant in this interval. And as follows from Eqs. (2) - (3), both the potential and kinetic energies are independent of the liquid compressibility. Thus in this interval the bubble wall motion is almost independent of the liquid compressibility and of any thermodynamic processes in the bubble or at the bubble wall. It follows then that the motion of the wall of any real bubble is well modeled by the present theory in this interval.

It does not mean that the thermodynamic processes in this interval play no role in the bubble wall motion. However, these processes will manifest themselves significantly only during the last 3% of the contraction phase. In other words, the processes that take place in the bubble and at the bubble wall in this interval are accumulating their effects to show them in full strength just in the last few moments of the bubble contraction, lasting only about 3% of the contraction phase. Only in these last instants an important information can be obtained (e.g., by observing the bubble wall motion) regarding the processes occurring in the whole contraction phase. And only such information can then serve as a solid base when defining a correct mathematical model of the real bubble.

In the last moments of the contraction phase, when the kinetic energy and partially also the remaining part of the potential energy are being intensively transformed into the internal energy of the gas, a part of these energies is being dissipated as the acoustic energy in the theoretical model. However, analysis of the experimental data shows [3, 26, 35 - 38] that in the real bubble a part of the potential and kinetic energy is dissipated not only as the acoustic energy, but also by some further, yet unknown processes. Therefore any further computation at the final stages of the bubble contraction and in the following expansion phase must be done (and interpreted) with utmost care, because the present theoretical model begins to depart from reality significantly.

Hence, if the computation continues further beyond the first contraction phase that is in the first expansion phase, a picture similar to that obtained above can be seen again. Now the flow of the energies is inverted. The energy accumulated in the gas as the internal energy is transformed extremely fast mainly into the kinetic energy of the liquid (now the liquid is streaming outwards the bubble), partially also into the potential energy of the bubble. In the theoretical model it is also partially dissipated as the acoustic energy, whereas in a real bubble it is dissipated as the acoustic energy and also (as already mentioned above) by some yet unknown processes. These initial transforms will last about 3% of the first expansion phase again. However, because a large part of the energies has been dissipated in the vicinity of the minimum radius R_{m1}, the magnitude of the kinetic and potential energies will be smaller now (see Fig. 3). At the end of this short interval the kinetic energy attains a maximum value and in the following long interval, lasting about 97% of the expansion phase, this kinetic energy and the remaining part of the internal energy are being transformed back into the potential energy of the bubble. And again, the energy transforms in this long interval are independent of the liquid compressibility and of the thermodynamic processes in the bubble and at the bubble wall. Resulting form of the radius vs. time curve will be the same as in the case of the first oscillation. However, now the size of the *R(t)* curve (characterized by the value of R_{M2}) will be smaller, because a large part of the energies has been dissipated during the bubble wall motion in the vicinity of the minimum radius R_{m1} (see Fig. 4).

From what has been said (and what can be seen in Fig. 3) it follows that both the contraction and expansion phases can be divided into two distinct intervals. The first interval, which includes about 97% of each phase, in which the governing energy transform is between the potential and kinetic energy, and the second interval, which includes about 3% of each phase, in which the governing energy transform is between the kinetic and internal energy. And in this small second interval a large part of the internal energy is dissipated as the acoustic energy (in the theoretical model) or as the acoustic energy and some other experimentally yet not sufficiently studied energies.

With respect to the governing energy transforms the first large interval can be called the PK interval ("*potential-kinetic*" interval), and the second small interval can be called the KI interval ("*kinetic-internal*" interval). In these abbreviations the acoustic energy has been omitted for the sake of simplicity.

It follows from the previous discussion that the shape of the *R(t)* curve is determined in the PK interval. The previous discussion also explains why this shape is independent of the liquid compressibility and of the thermodynamic processes in the bubble and at the bubble wall. On the other hand all important thermodynamic and dissipative processes will manifests their effects in the KI interval.

An instant the kinetic energy attains the maximum value will be denoted as t_k and it can be used as a suitable boundary point between the PK and KI intervals (see also Fig 3). The extent of the KI interval is then $\Delta t=T_{c1}-t_k$ and it may be convenient to express this extent as a percentage of the contraction phase duration, that is as $\delta_k=100\Delta t/T_{c1}$. It is evident that the value of δ_k also depends on the bubble oscillation intensity. Thus for $A_1=2.6$ (medium intensity oscillations) is obtained $\delta_k=5.9\%$, for $A_1=3$ is obtained $\delta_k=4.0\%$, and for $A_1=3.4$ (high intensity oscillations) is obtained $\delta_k=2.9\%$. These values of δ_k have been computed with the bubble model described above.

It is possible to define similar intervals as above for the first expansion phase as well. One will obtain the IK ("*internal-kinetic*") and KP ("*kinetic-potential*") intervals now.

The discussion of the energy transforms in a freely oscillating bubble just presented also explains why the value of T_{c1} is only very weakly dependent on the bubble oscillation intensity, liquid compressibility, the thermodynamic processes in the bubble interior and at the bubble wall (e.g., whether the bubble interior contains gas or vapor), and on the dissipative processes accompanying the bubble oscillations. In other words, the discussion reveals why T_{c1} determined in the classical Rayleigh's model of an empty bubble fits so well the experimental data, and also why, when measuring in experiments only T_{c1}, not much can be learned about the observed bubble.

DISCUSSION

In Sections 1 and 2 it has been shown that by observing the bubble wall motion in the PK and KP intervals nothing significant can be obtained about the bubble (with the exception of the maximum radii R_{M1} and R_{M2}). In case of bubbles oscillating sufficiently intensively, the shape of the curves *R(t)* in the first and second oscillations, apart from the size, is almost the same. This is true for both the gas and vapor bubbles, that is, not only for spark and laser generated bubbles, but also for cavitation bubbles (generated both in hydrodynamic and acoustic cavitation) and for bubbles generated by underwater chemical explosions. By observing this shape no conclusion about liquid evaporation or vapor condensation, gas diffusion, heat conduction etc. can be made. If the bubble oscillation intensity is specified properly, all bubble models commonly used (Rayleigh's, Herring's, Herring's modified, Gilmore's, etc.) yield almost the same variation of the bubble radius with time in these intervals (see Fig. 2). This very good fitting of all bubble models to the experimental data testifies that any unaccounted for process in the PK and KP intervals has a negligible effect on the shape of the *R(t)* curve. If the intention is to learn more about the bubble or to verify the validity of a theoretical model, then the bubble wall motion must be observed in the KI and IK intervals first of all and the study of the wall motion must always be accompanied by investigation of other processes (such as the acoustic and optic radiations from the bubble) as well.

So far, only a limited number of "probes" into the IK and KI intervals have been reported in the literature [27, 28]. Since the knowledge of bubble behavior in the IK and KI intervals is severely limited at present, it cannot be decided by comparing the experiments with theory which mathematical model (Gilmore's, Herring's, etc.) gives the best results. Therefore at present time it is rather irrelevant which bubble model is used for the analysis. This is also one of the reasons why the Herring's modified model is used in this work.

As said above, for bubbles oscillating sufficiently intensively the shape of the radius vs. time curves will always be the "inverted tea cup", both in the first and second bubble oscillation. The size of the *R(t)* curve in the first oscillation will be determined by the energy available for the growth phase minus energy dissipated at the initial instance of the bubble growth (the growth phase of spark generated bubbles has not been discussed in this paper). The size of the *R(t)* curve in the second oscillation will depend on the energies remaining from the first oscillation after the dissipated energies are subtracted. Thus in the graphical presentation of the first and second bubble oscillations there are always two "inverted tea cups" next to each other. First, a larger "cup" corresponding to the first bubble oscillation, followed by a smaller "cup" corresponding to the second bubble oscillation (for the sake of brevity further bubble oscillations are omitted from the discussion). How small the second "cup" is, as compared with the first one depends on the energy dissipated in the KI and IK intervals first of all. However, it follows from the results presented in Section 2 that as far as the shape of the *R(t)* curve and its size are concerned, the nature of the dissipative mechanism (whether it is the acoustic radiation, thermal radiation, heat conduction, liquid evaporation, vapor condensation, etc.) plays no role. As can be verified in literature, this fact is very often ignored and this leads to misinterpretation of the measured data.

Because at present the role of the different dissipative processes has not been clarified yet (and thus these processes cannot be included in the respective theoretical models correctly), some researchers try to fit the size of the *R(t)* curve in the second oscillation by using the dissipative mechanisms already known. These are, first of all, the acoustic radiation, and in case of smaller bubbles also the viscosity losses (which are unimportant for the large bubbles considered here). The amount of the radiated acoustic energy increases with the bubble oscillation intensity. Thus by increasing the bubble oscillation intensity A_1 sufficiently, the required cumulative dissipated energy can be obtained and thus also the required fit to the experimentally determined size of the *R(t)* curve in the second oscillation can be achieved. Such a procedure is shown in Fig 4.

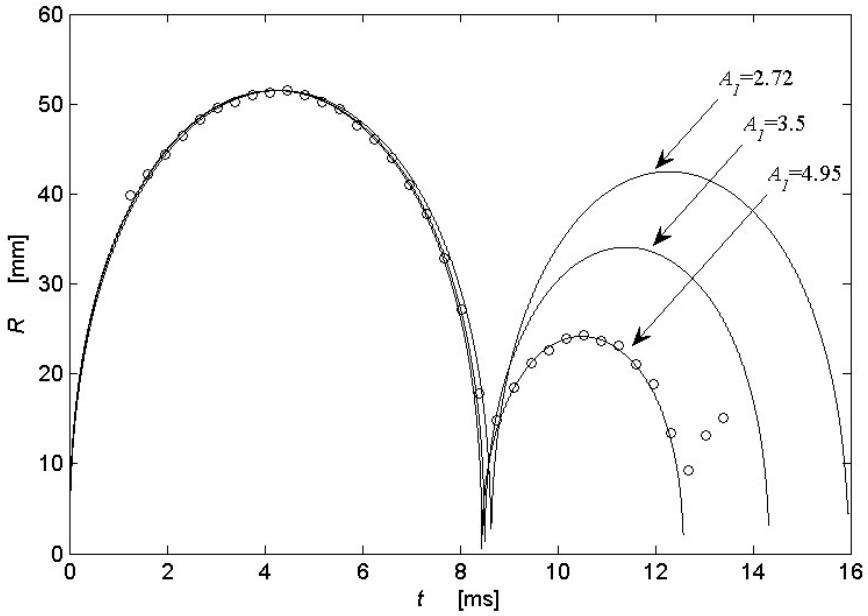

Fig. 4 Fitting the experimental data with theoretical curves computed for different bubble oscillation intensities A_1. The time scale origin is set at the beginning of the growth phase. The experimental data originate from the same experiment as those shown in Fig. 2. However, now all the experimental data available both for the first growth phase, the first contraction phase and the second and third oscillations are displayed. The theoretical variations of R with t have been computed with Herring's modified model starting at R_{M1} and the growth phases have been obtained by inverting the first contraction phases. The physical constants and parameters used in computations are given in Section 1

In Fig. 4 the amplitude A_1=2.72 corresponds to the bubble oscillation intensity determined from the measured peak pressure in the first acoustic pulse, that is from p_{zp1}=70.3. Because only acoustic losses are present in Herring's modified model and these are relatively small for this oscillation intensity, the computed second maximum radius R_{M2} is relatively large. The amplitude A_1=4.95 represents the bubble oscillation intensity needed to fit the experimental data also in the second oscillation. Now the acoustic radiation is sufficient to cover all the losses occurring in a real bubble. However, such an approach is not correct because in real bubbles other dissipative mechanisms are also present. And it must be stressed here that the bubble oscillation intensity used to fit the experimental data is excessively high now and this may lead to incorrect physical results.

To illustrate possible pitfalls arising from using the excessive bubble oscillation intensities, let us have a look at the density ρ of the gas in a theoretical bubble. Assuming the conservation of the mass in an ideal gas bubble (such assumption is implicitly present in Eq. (4)) it follows that $(4/3)\pi R_e^3 \rho_e = (4/3)\,\pi R_{m1}^3 \rho_{m1}$. Here ρ_e is the gas density at the equilibrium radius R_e and ρ_{m1} is the gas density at the first minimum radius R_{m1}. This equation can be rearranged easily to yield $\rho_{m1}=\rho_e(A_1\, Z_{m1})^{-3}$, where $Z_{m1}=R_{m1}/R_{M1}$. For the given amplitude A_1, the value of Z_{m1} can be computed using, e.g., the Herring's modified model. Thus for a bubble oscillating with the amplitude A_1=2.72 (this is the intensity of oscillation determined from p_{zp1} earlier) one obtains Z_{m1}=0.054. Assuming further that ρ_e=0.6 kg.m^{-3} (approximately the density of saturated vapor at the pressure p_∞=100 kPa and temperature Θ=100 °C), then ρ_{m1}=189 kg.m^{-3}. For A_1=4.95 (this is the bubble oscillation intensity used in Fig 4 to fit the experimental data both in the contraction and expansion phases) one obtains $Z_{m1}\approx$0.0125, and hence $\rho_{m1}\approx 2.5 \times 10^3$ kg.m^{-3}. However, if the computation is done with Gilmore's model as it is common in the literature, then to obtain a fit to the second maximum bubble radius R_{M2}, the bubble oscillation intensity must be increased from A_1=4.95 to A_1=5.78 (Gilmore's model radiates acoustically less intensively than Herring's modified model and therefore higher A_1 is needed now). In this case the corresponding value of the non-dimensional minimum radius is $Z_{m1}\approx$0.0033 and the density is $\rho_{m1}\approx 86 \times 10^3$ kg.m^{-3}. Let us remind here that the highest densities of solids given in physical tables are approximately $\rho\approx$20

x 10^3 kg.m^3 (e.g., for tungsten ρ=19.3 x 10^3 kg.m^3). To emphasize the fact that the computed values of Z_{m1} and ρ_{m1} are physically unrealistic, the signs "almost equal to" have been used here.

It can be seen immediately that the value of ρ_{m1} obtained with the Gilmore's model is unrealistically high from the physical point of view. However, when reviewing the literature on bubble oscillations, numerous examples of computations can be found where the authors use similar extremely high values of bubble oscillation intensity in order to obtain the required fit to the experimental data (this approach has been used by Lauterborn and his students first [34], and it is extensively used in theoretical computations on bubbles oscillating in acoustic resonators nowadays). Such a procedure is possible because from the mathematical point of view there is no limit on the theoretical bubble oscillation intensity. To solve the problem concerning these excessive gas densities, some authors have been considering the so called van der Waals hard core. However, this is a cosmetic procedure only, which cannot overcome the physical incorrectness caused by not considering all dissipative processes existing in a bubble. In real bubbles these dissipative processes "soften" the bubble oscillations significantly so that the usage of van der Waals core in theoretical computations is then most probably unnecessary (see the value of ρ_{m1} computed above for the intensity of oscillation A_1=2.72).

CONCLUSIONS

At the beginning of Section 2 a number of simplifying assumptions have been made. These assumptions concerned, e.g., the liquid compressibility, the thermal behavior of the bubble, and the method of the bubble excitation for free oscillation. In the following analysis it has been verified that in the PK and KP intervals these assumptions play, if any, then only a minor role. However, in the KI and IK intervals these assumptions cannot be used. Nevertheless, the analysis in the KI and IK intervals has been purposefully limited to a minimum, with the exception of a few points discussed in Section 3.

It has been shown that by observing the bubble wall motion in the PK and KP intervals only, not much information about the processes in a bubble can be obtained. This fact certainly represents a serious limit regarding the correct formulation of a bubble model. Thus it is not possible to agree with the authors of the recent review paper [34], who claim that "a remarkable agreement can be obtained" between experimental points and theoretical computations based on Keller-Miksis model (cf. a remark at Fig. 38 of Ref. [34]). In this case the theoretical bubble oscillates with the amplitude $A_1=R_{max}/R_n$=10.8 (the nomenclature used in Ref. [34] for R_{M1} and R_e has been adopted here). As far as the density ρ_{m1} at such high oscillation intensities is concerned, we refer to the numerical examples given in Section 3. Unfortunately, similar procedures, which are based on using excessive and unrealistic intensities of bubble oscillation, are very common in literature.

It is our opinion that to obtain a better understanding of the bubble behavior a lot of work still must be done. New experiments should concentrate on the bubble wall motion in the KI and IK intervals first of all. For example, it is already known that the bubble shape at the final stages of the contraction phase is not spherical [27,28]. However, no further details of this shape are known. And the observations of the bubble wall motion must always be accompanied by measurements of the acoustic and optic radiation and by studying other processes as well. This is a very challenging task. However, no further progress in the correct understanding of bubble oscillations can be obtained without completing this target.

ACKNOWLEDGEMENT

This work has been supported by the Ministry of Education of the Czech Republic as the research project MSM 245 100 304. The author also wishes to thank Dr. Silvano Buogo from the Italian Acoustics Institute, CNR, Rome, Italy, for a very valuable help with taking the high-speed camera records.

REFERENCES

[1] JAYAPRAKASH A., HSIAO C.-T. and CHAHINE G. Numerical and experimental study of the interaction of a spark-generated bubble and a vertical wall [J]. **Transactions of the ASME, Journal of Fluid Engineering,** 2012, 134(3): 031301.

[2] SHAW S.J., SCHIFFERS W.P. and EMMONY D.C. Experimental observation of the stress experienced by a solid surface when a laser-created bubble oscillates in its vicinity [J]. **Journal of the Acoustical Society of America,** 2001, 110(4): 1822-1827.

[3] ISSELIN J.-C., ALLONCLE A.-P. and AUTRIC M. On laser induced single bubble near a solid boundary: Contribution to the understanding of erosion phenomena [J]. **Journal of Applied Physics,** 1998, 84(10): 5766-5771.

[4] WANG Q.-X., YANG Y.-X., TAN D.S., SU J. and TAN S.K. Non-spherical multi-oscillations of a bubble in a compressible liquid [J]. **Journal of Hydrodynamics**, 2014, 26(6): 848-855.

[5] YANG Y.X., WANG Q.X. and KEAT T.S. Dynamic features of a laser-induced cavitation bubble near a solid boundary [J]. **Ultrasonics Sonochemistry**, 2013, 20(4): 1098-1103.

[6] SBOROS V. Response of contrast agents to ultrasound [J]. **Advanced Drug Delivery Reviews,** 2008, 60(10): 1117-1136.

[7] STRIDE E.P. and COUSSIOS C.C. Cavitation and contrast: the use of bubbles in ultrasound imaging and therapy [J]. **Proceedings of the Institution of Mechanical Engineers Part H-Journal of Engineering in Medicine,** 2010, 224(42): 171-191.

[8] THOMAS D.H., BUTLER M., PELEKASIS N., ANDERSON T., STRIDE E. and SBOROS V. The acoustic signature of decaying resonant phospholipid microbubbles [J]. **Physics in Medicine and Biology,** 2013, 58(3): 589-599.

[9] FAEZ T., EMMER M., KOOIMAN K., VERSLUIS M., VAN DER STEAN A.F.W. and DE JONG N. 20 years of ultrasound contrast agent modeling [J]. **IEEE Transactions on Ultrasonics Ferroelectrics and Frequency Control,** 2013, 60(1): 7-20.

[10] LEIGHTON T.G., TURANGAN C.K., JAMALUDDIN A.R., BALL G.J. and WHITE P.R. Prediction of far-field acoustic emissions from cavitation clouds during shock wave lithotripsy for development of a clinical device [J]. **Proceedings of the Royal Society A-Mathematical Physical and Engineering Sciences**, 2013, 469(2165): 20120538.

[11] KANG G., CHO S.C., COLEMAN A.J. and CHOI M.J. Characterization of the shock pulse-induced cavitation bubble activities recorded by an optical fiber hydrophone [J]. **Journal of the Acoustical Society of America,** 2014, 135(3): 1139-1148.

[12] DE GRAAF K.L., BRANDNER P.A. and PENESIS I. Bubble dynamics of a seismic airgun [J]. **Experimental Thermal and Fluid Science,** 2014, 55: 228-238.

[13] DE GRAAF K.L., BRANDNER P.A. and PENESIS I. The pressure filed generated by a seismic airgun [J]. **Experimental Thermal and Fluid Science,** 2014, 55: 239-249.

[14] DE GRAAF K.L., PENESIS I. and BRANDNER P.A. Modelling of seismic airgun bubble dynamics and pressure field using the Gilmore equation with additional damping factors [J]. **Ocean Engineering,** 2014, 76: 32-39.

[15] HUSIN S., ADDALI A. and MBA D. Observation of acoustic emission from gas bubble inception and burst [J]. **Proceedings of the Institution of Mechanical Engineers Part E-Journal of Process Mechanical Engineering**, 2012, 226(E1): 79-78.

[16] WU X., CHOI J.-K., SINGH S., HSIAO C.-T. and CHAHINE G.L. Experimental and numerical investigation of bubble augmented waterjet propulsion [J]. **Journal of Hydrodynamics**, 2012, 24(5): 635-647.

[17] ZHANG Y.-N. and LI S.-C. Effects of liquid compressibility on radial oscillations of gas bubbles in liquids [J]. **Journal of Hydrodynamics**, 2012, 24(5): 760-766.

[18] FOUAN D., ACHAOUI Y., PAYAN C. and MENSAH S. Microbubble dynamics monitoring using a dual modulation method [J]. **Journal of the Acoustical Society of America,** 2015, 137(2): EL144-EL150.

[19] IWATA Y., TAKADA N. and SASAKI K. A simple method for efficient generation of standing cavitation bubbles [J]. **Applied Physics Express**, 2013, 6(12): 127301.

[20] GEERS T.L. Optimization of an augmented Prosperetti-Lezzi bubble model [J]. **Journal of the Acoustical Society of America,** 2014, 136(1): 30-36.

[21] BUOGO S. and CANNELLI G.B. Implosion of an underwater spark-generated bubble and acoustic energy evaluation using the Rayleigh model [J]. **Journal of the Acoustical Society of America,** 2002, 111(9): 2594-2600.

[22] KRIEGER J.R. and CHAHINE G.L. Acoustic signals of underwater explosions near surfaces [J]. **Journal of the Acoustical Society of America,** 2005, 118(5): 2961-2974.

[23] KHOO B.C., ADIKHARI D., FONG S.W. and KLASEBOER E. Multiple spark-generated bubble interactions [J]. **Modern Physics Letters B**, 2009, 23(3): 229-232.

[24] FONG S.W., ADHIKARI D., KLASEBOER E. and KHOO B.C. Interactions of multiple spark-generated bubbles with phase differences [J]. **Experiments in Fluids,** 2009, 46(4): 705-724.

[25] HUANG Y., YAN H., WANG B., ZHANG X., LIU Z. and YAN K. The electro-acoustic transition process of pulsed corona discharge in conductive water [J]. **Journal of Physics D: Applied Physics**, 2014, 47(25): 255204.

[26] WARD B. and EMMONY D.C. Interferometric studies of the pressures developed in a liquid during infrared-laser-induced cavitation-bubble oscillation [J]. **Infrared Physics,** 1991, 32: 489-515.

[27] BAGHDASSARIAN O., CHU H.-C., TABBERT B. and WILLIAMS G.A. Spectrum of luminescence from laser-created bubbles in water [J]. **Physical Review Letters,** 2001, 86(21): 4934-4937.

[28] LINDAU O. Investigation of laser generated cavitation (Untersuchungen zur lasererzeugten Kavitation) [D]. Ph.D. Dissertation, Universität Göttingen 2001 (published at: Der Andere Verlag, 49074 Osnabrück, Germany, ISBN: 3-935316-49-6). (In German).

[29] GREGORČIČ P., JEZERŠEK M. and MOŽINA J. Optodynamic energy-conversion efficiency during an Er:YAG-laser-pulse delivery into a liquid through different fiber-tip geometries [J]. **Journal of Biomedical Optics,** 2012, 17(7): 075006.

[30] OBRESCHKOW D., TINGUELY M., DORSAZ N., KOBEL P., DE BOSSET A. and FARHAT M. The quest for the most spherical bubble: experimental setup and data overview [J]. **Experiments in Fluids,** 2013, 54(4): 1503.

[31] HEGEDÜS F., KOCH S., GAREN W., PANDULA Z., PAÁL G., KULLMANN L. and TEUBNER U. The effect of high viscosity on compressible and incompressible Rayleigh-Plesset-type bubble models [J]. **International Journal of Heat and Fluid Flow,** 2013, 42: 200-208.
[32] BULANOV A.V., NAGORNYI I.G. and SOSEDKO E.V. Specific features of the acoustic emission upon the optical breakdown in liquid induced by the radiation of Nd:YAG laser [J]. **Technical Physics**, 2013, 58(8): 1201-1204.
[33] SATO T., TINGUELY M., OIZUMI M. and FARHAT M. Evidence for hydrogen generation in laser- or spark-induced cavitation bubbles [J]. **Applied Physics Letters**, 2013, 102: 074105.
[34] LAUTERBORN W. and KURZ T. Physics of bubble oscillations [J]. **Reports on Progress in Physics,** 2010, 73(10): 106501.
[35] BUOGO S., PLOCEK J. and VOKURKA K. Efficiency of energy conversion in underwater spark discharges and associated bubble oscillations: Experimental results [J]. **Acta Acustica united with Acustica,** 2009, 95(1): 46-59.
[36] BUOGO S. and VOKURKA K. Intensity of oscillation of spark-generated bubbles [J]. **Journal of Sound and Vibrations,** 2010, 329(20): 4266-4278.
[37] VOKURKA K. and PLOCEK J. Experimental study of the thermal behavior of spark generated bubbles in water [J]. **Experimental Thermal and Fluid Science,** 2013, 51: 84-93.
[38] VOKURKA K. Amplitudes of free bubble oscillations in liquids [J]. **Journal of Sound and Vibration,** 1990, 141(2): 259-275.
[39] VOKURKA K. Comparison of Rayleigh's, Herring's, and Gilmore's models of gas bubbles [J]. **Acustica**, 1986, 59(3), 214-219.